Since January 2020 Elsevier has created a COVID-19 resource centre with free information in English and Mandarin on the novel coronavirus COVID-19. The COVID-19 resource centre is hosted on Elsevier Connect, the company's public news and information website.

THE JOURNAL OF BIOLOGICAL CHEMISTRY
Vol. 279, No. 17, Issue of April 23, pp. 17996–18007, 2004
Printed in U.S.A.

ACE2 X-Ray Structures Reveal a Large Hinge-bending Motion Important for Inhibitor Binding and Catalysis*

Received for publication, October 10, 2003, and in revised form, January 26, 2004
Published, JBC Papers in Press, January 30, 2004, DOI 10.1074/jbc.M311191200

Paul Towler‡, Bart Staker§, Sridhar G. Prasad§¶, Saurabh Menon‡, Jin Tang‖, Thomas Parsons‖, Dominic Ryan‡, Martin Fisher‡, David Williams‡, Natalie A. Dales‡, Michael A. Patane‡, and Michael W. Pantoliano‡**

From ‡Drug Discovery and ‖Protein Sciences, Millennium Pharmaceuticals, Incorporated, Cambridge, Massachusetts 02139 and §Emerald BioStructures, Incorporated, Bainbridge Island, Washington 98110

The angiotensin-converting enzyme (ACE)-related carboxypeptidase, ACE2, is a type I integral membrane protein of 805 amino acids that contains one HE*XX*H + E zinc-binding consensus sequence. ACE2 has been implicated in the regulation of heart function and also as a functional receptor for the coronavirus that causes the severe acute respiratory syndrome (SARS). To gain further insights into this enzyme, the first crystal structures of the native and inhibitor-bound forms of the ACE2 extracellular domains were solved to 2.2- and 3.0-Å resolution, respectively. Comparison of these structures revealed a large inhibitor-dependent hinge-bending movement of one catalytic subdomain relative to the other (~16°) that brings important residues into position for catalysis. The potent inhibitor MLN-4760 ((*S*,*S*)-2-{1-carboxy-2-[3-(3,5-dichlorobenzyl)-3*H*-imidazol4-yl]-ethylamino}-4-methylpentanoic acid) makes key binding interactions within the active site and offers insights regarding the action of residues involved in catalysis and substrate specificity. A few active site residue substitutions in ACE2 relative to ACE appear to eliminate the S_2' substrate-binding subsite and account for the observed reactivity change from the peptidyl dipeptidase activity of ACE to the carboxypeptidase activity of ACE2.

The angiotensin-converting enzyme (ACE)[1]-related carboxypeptidase, ACE2, is a type I integral membrane protein of 805 amino acids that contains one HE*XX*H + E zinc-binding consensus sequence (1, 2). The catalytic domain of ACE2 is 42% identical to that of its closest homolog, somatic angiotensin-converting enzyme (sACE; EC 3.4.15.1), a peptidyl dipeptidase that plays an important role in the renin angiotensin system for blood pressure homeostasis. The loss of ACE2 in knockout mice has no effect on blood pressure, but reveals ACE2 as an essential regulator of heart function (3). In a recent discovery, ACE2 was identified as a functional receptor for the coronavirus that is linked to the severe acute respiratory syndrome (SARS) (4, 5).

The physiological differences observed in the phenotypes of ACE (6, 7) and/or ACE2 (3) knockout mice presumably reflect the significant differences in substrate specificity and reactivity between these enzymes. Many substrates for ACE2 were identified by screening biologically active peptides (8). In all cases, only carboxypeptidase activity was found. Of the seven best *in vitro* peptide substrates identified ($k_{cat}/K_m > 10^5$ M^{-1} s^{-1}), proline and leucine are the preferred P_1 residues, with a partiality for hydrophobic residues in the P_1' position, although basic residues at P_1' are also cleaved (peptide-binding subsites in proteins are as previously defined (9)). Some of the best *in vitro* peptide substrates are apelin-13, des-Arg^9-bradykinin, angiotensin II, and dynorphin A-(1–13). The longest peptide substrate identified is a 36-residue peptide, apelin-36 (8). An examination of the ACE2 and ACE literature may be found in recently published reviews (10–12).

We report here the first crystal structures of the extracellular metallopeptidase domain of ACE2 in its native and inhibitor-bound states and discuss the influence of these structures in understanding the substrate specificity and catalytic mechanism of the enzyme. While preparing these ACE2 structures for publication, two reports on the crystal structures of testicular angiotensin-converting enzyme (tACE) and *Drosophila* ACE appeared in the literature (13, 14).

EXPERIMENTAL PROCEDURES

Protein Expression and Purification—A truncated extracellular form of human ACE2 (residues 1–740) was expressed in baculovirus and purified as described previously (8). The signal sequence (residues 1–18) is presumably removed upon secretion from Sf9 cells. The molecular mass of the purified enzyme is 89.6 kDa by matrix-assisted laser desorption ionization time-of-flight mass spectrometry, which is greater than the theoretical molecular mass of 83.5 kDa expected from the sequence (residues 19–740). The difference of ~6 kDa is believed to be due to glycosylation at the seven predicted *N*-linked glycosylation sites for this protein.

Crystallization—Briefly, 2 μl of purified ACE2 (5 mg/ml) was combined with an equal volume of reservoir solution, and crystals were grown by hanging drop vapor diffusion at 16–18 °C. The best crystallization reservoir solution conditions for native ACE2 were found to be 100 mM Tris-HCl (pH 8.5), 200 mM $MgCl_2$, and 14% polyethylene glycol 8000. Under these conditions, it took ~2 weeks to grow single crystals suitable for x-ray diffraction. Similarly, diffraction-quality ACE2 crystals were also grown in the presence of an ACE2 inhibitor, MLN-4760 (ML00106791; (*S*,*S*)-2-{1-carboxy-2-[3-(3,5-dichlorobenzyl)-3*H*-imidazol-4-yl]-ethylamino}-4-methylpentanoic acid). Compound MLN-4760 corresponds to compound 16 of Dales *et al.* (15). Crystallization trials used 2 μl of reservoir solution plus 2 μl of ACE2 at 5.9 mg/ml containing 0.1 mM inhibitor. The best diffracting ACE2-inhibitor complex crystals were grown in the presence of 19% polyethylene glycol 3000, 100 mM Tris-HCl (pH 7.5), and 600 mM NaCl.

Data Collection and Structure Determination—The best data set for

* The costs of publication of this article were defrayed in part by the payment of page charges. This article must therefore be hereby marked "*advertisement*" in accordance with 18 U.S.C. Section 1734 solely to indicate this fact.

The atomic coordinates and structure factors (code 1R42 and 1R4L) have been deposited in the Protein Data Bank, Research Collaboratory for Structural Bioinformatics, Rutgers University, New Brunswick, NJ (http://www.rcsb.org/).

¶ Present address: Syrrx Inc., San Diego, CA 92121.

** To whom correspondence should be addressed: Millennium Pharmaceuticals, Inc., 270 Albany St., Cambridge, MA 02139. Tel.: 617-551-8677; Fax: 617-551-7919; E-mail: pantoliano@mpi.com.

[1] The abbreviations used are: ACE, angiotensin-converting enzyme; sACE, somatic angiotensin-converting enzyme; tACE, testicular or germinal angiotensin-converting enzyme; SARS, severe acute respiratory syndrome; r.m.s., root mean square; Z, benzyloxycarbonyl.

TABLE I
Heavy atom data statistics for human native ACE2

*p*CMB, *p*-chloromercuribenzoate; PIP, di-μ-iodobis(ethylenediamine) diplatinum(II) nitrate; NA, not applicable.

Derivative	Native (Zn)	*p*CMB	$HgCl_2$	PIP	K_2PtCl_4
Heavy atom	Zn	Hg	Hg	Pt	Pt
Molarity (mM)	NA	1	1	1	1
Length of soak (day(s))	NA	3.5	30	1	30
No. sites/asymmetric unit[a]	1	1	1	2	2
Wavelength (Å)[b]	1.2824	1.009	1.009	1.072	1.072
Unique reflections	49,286[c]	21,652[c]	17,421	13,152	14,087
Resolution (Å)	40–2.2	30–2.9	30–3.0	30–3.4	30–3.3
Completeness (%)	96.3	96.6	90.6	95.4	94.2
R_{sym} (%)[d]	5.7	10.5	10.4	9.7	11.6
R_{merge}[e]	NA	21.3	37.6	20.6	21.8
R_{cullis}[f]	0.94	0.73	0.93	0.96	0.97
Phasing power[g]	1.57	1.51	0.66	0.45	0.39

[a] Each asymmetric unit contains one human ACE2 protein.
[b] Data were collected at the Brookhaven National Laboratory (NSLS, beam line X25) or at the Argonne National Laboratory (APS, beam line sector 32, COM-CAT). The wavelength for the native (zinc) data set was 1.2824 Å to maximize the anomalous signal at the zinc absorption edge.
[c] Values do not include Bijvoet pairs. Inclusion of Bijvoet pairs increases the number of reflections to 91,550 for native (zinc) ACE2 and 41,716 for the *p*-chloromercuribenzoate derivative.
[d] $R_{sym} = \Sigma|I_i - I_m|/\Sigma I_m$, where I_i is the intensity of the measured reflection and I_m is the mean intensity of all symmetry-related reflections.
[e] $R_{merge} = \Sigma|F_{PH} - F_P|/\Sigma|F_{PH}|$.
[f] $R_{cullis} = \Sigma|(F_{PH} \pm F_P) - F_{H(calc)}|/\Sigma|F_{PH} - F_P|$.
[g] Phasing power = F_H/E_{RMS}, where E_{RMS} is the residual lack of closure.

TABLE II
Refinement statistics for native and inhibitor-bound ACE2 structures

Numbers in parentheses represent final shell of data. PDB, Protein Data Bank.

	Native ACE2 (PDB code 1R42)	Inhibitor-bound ACE2 (PDB code 1R4L)
Resolution (Å)	46.7–2.20 (2.34–2.20)	43.3–3.0 (3.19–3.00)
No. reflections	47,465 (5982)	17,228 (2250)
R_{sym} (%)[a]	5.7 (40.8)	7.0 (20.4)
Completeness (%)	96.3 (81.8)	96.8 (85.1)
Space group	C2	C2
a	103.64	100.53
b	89.46	86.51
c	112.40	105.86
β	109.15	103.65
Unit cell volume (Å^3)	986,854	894,383
Solvent content (%)[b]	53	53
Molecules/asymmetric unit	1	1
Reflections used in R_{free}	4798	1723
No. protein atoms	5165	5147
No. solvent atoms	302	13
No. zinc atoms	1	1
No. chloride atoms	1	1
No. sugar atoms	42	28
R-factor (%)	23.5 (37.9)	25.3 (37.9)
R_{free} (%)	28.7 (39.8)	33.7 (46.0)
r.m.s. deviations from ideal stereochemistry		
Bond lengths (Å)	0.008	0.008
Bond angles	1.4°	1.5°
Dihedrals	21.7°	22.2°
Impropers	0.92°	0.97°
Mean *B*-factor (all atoms; Å^2)	59.9	74.5

[a] See Footnote *d* of Table I.
[b] $V_{solvent} = 1–1.23/V_m$, where V_m is the volume of protein in the unit cell/volume of unit cell, assuming one molecule/asymmetric unit and four asymmetric units in the monoclinic unit cell.

native ACE2 was at 2.2-Å resolution and was collected at the Advanced Photon Source (Argonne National Laboratory). A total of 44 x-ray data sets were collected for native ACE2, including a large number of heavy atom soaks of atoms that had good anomalous signals. The data sets for each derivative were collected at different wavelengths to maximize the anomalous signals for the bound heavy atoms. Native ACE2 data were collected to 2.2-Å resolution at $\lambda = 1.28$ Å to maximize the anomalous signal at the zinc absorption edge.

The heavy atom positions were determined and confirmed by a combination of visual inspection of Patterson maps and automatic search procedures, which included SHAKE 'N BAKE (16) and SHELXD (17). The heavy atom parameters were refined and optimized using the computer programs SHARP (18), MLPHARE (19), and XHEAVY (20). The experimental phases were improved by solvent flattening and histogram matching.

Once the native ACE2 structure was determined, it was used to solve the inhibitor-bound structure of ACE2 to 3.0-Å resolution using molecular replacement methods that employed the program AMoRe in the CCP4 software suite (21). The native structure was split into two subdomains: subdomains I and II (see Fig. 3 for definition). Subdomain II was used for molecular replacement and refined in REFMAC5, which resulted in the appearance of electron density for subdomain I. Subdomain I was then fitted into the density by hand, and the structure was refined as a whole. Final refinement was accomplished using the software suite CNX (22).

RESULTS AND DISCUSSION

Native ACE2 Structure—The three-dimensional structure of the extracellular region of native ACE2 was determined by multiple isomorphous replacement with anomalous scattering and refined to a crystallographic *R*-factor of 23.5% (R_{free} =

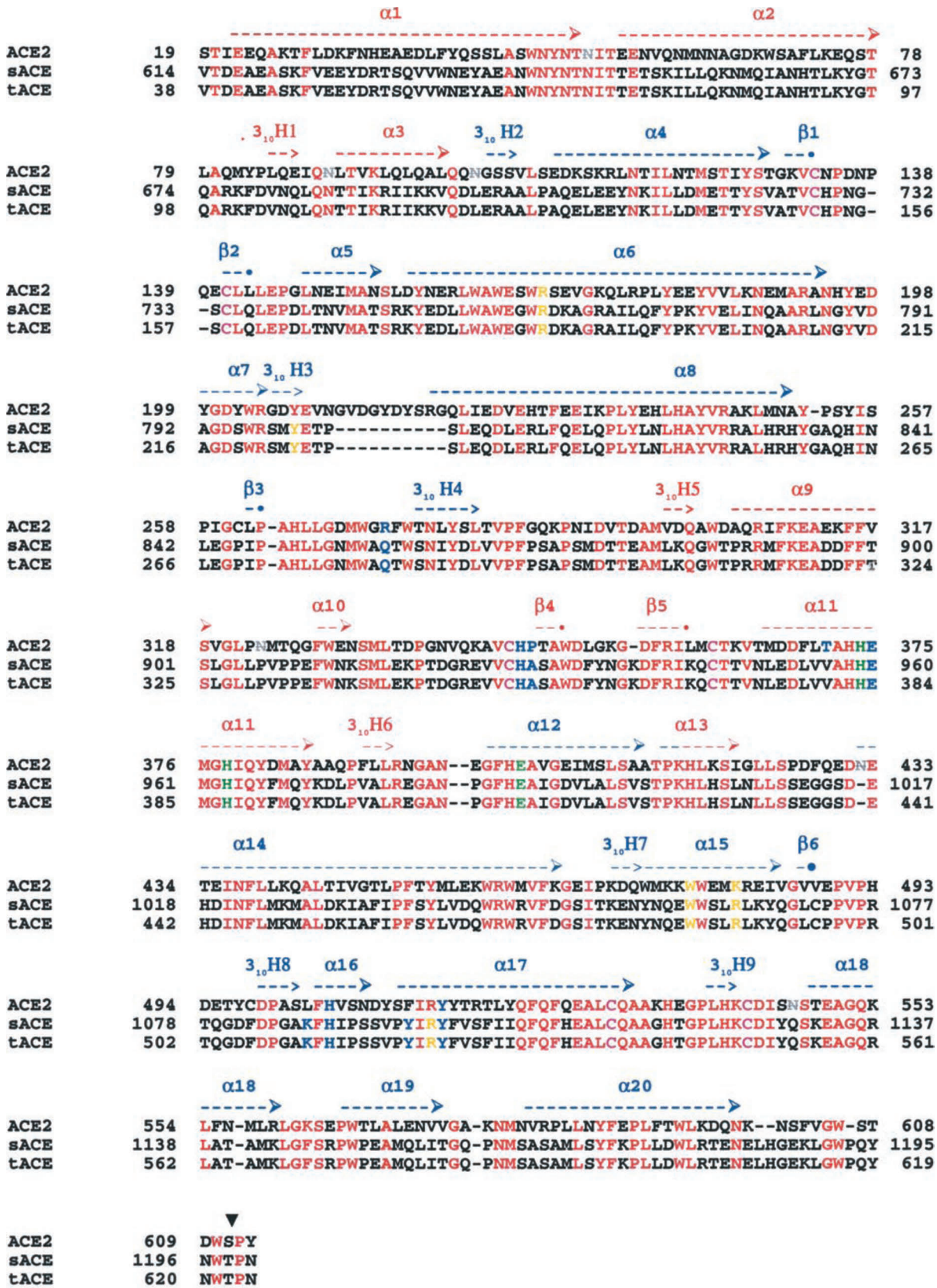

FIG. 1. **Sequence alignment of the metallopeptidase domains of human ACE2, sACE, and tACE.** The sequences of the catalytic domain of tACE and the C-terminal catalytic domain of sACE are identical (48, 49). The human sACE and ACE2 sequences were obtained from the GenBank™/EBI Data Bank (accession numbers P12821 and AAF99721, respectively). The ClustalW Alignment Tool was used for these sequence alignments (50). The secondary structural elements for native ACE2 were assigned using STRIDE software (51) and are denoted as follows: α-helical segments, – – ➢; 3_{10} helical elements, – – >; and β-structural segments, – – ●. These secondary structural elements are color-coded *red* for subdomain I and *blue* for subdomain II (subdomains are defined in Fig. 3). Identical residues for all three enzymes are colored *red*. The zinc-binding residues in all three enzymes are shown in *green*, and the chloride ion-binding residues in all enzymes are shown in *orange*. Residues in ACE2 within H-bonding distance of the inhibitor MLN-4760 or in tACE within H-bonding distance of lisinopril are colored *blue* (13). The Cys residues conserved between ACE2 and ACE are colored *magenta*. The six predicted *N*-linked glycosylation sites for the metallopeptidase region of ACE2 are shown (*gray N*). The beginning of the collectrin homology domain (23) in ACE2 is indicated (▼).

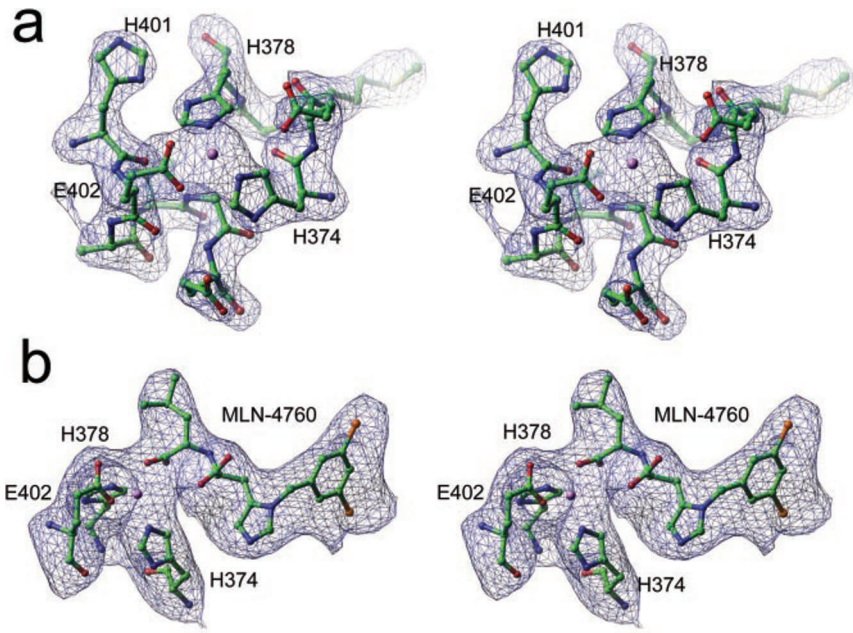

FIG. 2. **Experimental electron density maps for native and inhibitor-bound ACE2 structures.** *a*, an $|F_o| - |F_c|$ omit electron density map of the zinc-binding site of the native ACE2 structure (His^{374}–His^{378}, His^{401}–Glu^{406}), calculated with phases from the refined model at 2.2-Å resolution. The map is contoured at 3σ. *b*, an $|F_o| - |F_c|$ omit electron density map of MLN-4760, zinc, and the three metal-binding ligands of the protein (His^{374}, His^{378}, and Glu^{402}), calculated with phases from the refined model at 3.0-Å resolution. The map is contoured at 3σ.

28.7%) at 2.2-Å resolution. The heavy atom data statistics are summarized in Table I, and the refinement statistics for native ACE2 are summarized in Table II.

The extracellular region of the human ACE2 enzyme is composed of two domains. The first is a zinc metallopeptidase domain (residues 19–611), which is ~42% identical to the corresponding domains of human sACE and tACE (Fig. 1). Electron density near the active site of native ACE2 is shown in Fig. 2*a*. An α-carbon trace for this metallopeptidase domain of ACE2 is shown in Fig. 3*A*. The second domain is located at the C terminus (residues 612–740) and is ~48% identical to human collectrin (23). Unfortunately, the electron density map for much of the collectrin homology domain is weak. Only half of this domain is visible in the electron density map, and what can be seen is ambiguous due to topology and connectivity issues.

The metallopeptidase domain of ACE2 can be further divided into two subdomains (I and II) (Fig. 3*B*), which form the two sides of a long and deep cleft with dimensions of ~40 Å long by ~15 Å wide by ~25 Å deep. The two catalytic subdomains are connected only at the floor of the active site cleft. One prominent α-helix (helix 17, residues 511–531) connects the two subdomains and forms part of the floor of the canyon. The deeply recessed and shielded proteolytic active site of ACE2 is a common structural feature of proteases and exists to avoid hydrolysis of correctly folded and functional proteins (24, 25) and is also consistent with the profiles of binding of tethered inhibitors to sACE (26, 27).

The N terminus-containing subdomain I and the C terminus-containing subdomain II are defined in Fig. 3*B*. This subdomain definition is based on the subdomain movement that was observed upon inhibitor binding (see below). The secondary structure of the metallopeptidase domain of ACE2 is composed of 20 α-helical segments and nine 3_{10} helical segments that together make up ~62% of the structure (Figs. 1 and 3). This contrasts with just six short β-structural segments that make up ~3.5% of the structure. Glycosylation is suggested by the presence of electron density at all six potential *N*-linked sites: Asn^{53}, Asn^{90}, Asn^{103}, Asn^{322}, Asn^{432}, and Asn^{546} (2). The highest density was observed at Asn^{90}, Asn^{103}, and Asn^{546} and allowed the building of three *N*-acetylglucosamine groups. Three disulfide bonds of ACE2 (Cys^{133}–Cys^{141}, Cys^{344}–Cys^{361}, and Cys^{530}–Cys^{542}) are conserved in sACE and tACE (Fig. 1).

The zinc-binding site is located near the bottom and on one side of the large active site cleft (subdomain I side), nearly midway along its length. The zinc is coordinated by His^{374}, His^{378}, Glu^{402}, and one water molecule (in the native structure). These residues at the zinc-binding site of ACE2 make up the HE*XX*H + E motif conserved in the zinc metallopeptidase clan MA (28).

A chloride ion (Cl^-) is bound in native ACE2, coordinated by Arg^{169}, Trp^{477}, and Lys^{481} in subdomain II. The larger electron density compared with water supports the assignment of this density to a Cl^- ion, as does as the larger than expected distances between the coordinating side chains and the Cl^- ion (compared with water H-bonds): N-ϵ and N-η1 of Arg^{169} are both 3.2 Å from Cl^-, indole ring nitrogen of Trp^{477} is 3.5 Å from Cl^-, and N-ϵ of Lys^{481} is 5.0 Å from Cl^-.

Inhibitor-bound ACE2 Structure—The structure of ACE2 with an inhibitor bound at the active site was solved by molecular replacement to a resolution of 3.0 Å using the native ACE2 structure. Refinement statistics for the inhibitor-bound ACE2 structure are shown in Table II. The bound compound MLN-4760 potently inhibits human ACE2 (IC_{50} = 0.44 nM), but weakly inhibits tACE ($IC_{50} > 100$ μM) and carboxypeptidase A (IC_{50} = 27 μM) (15). The structure of the bound inhibitor is shown in Fig. 2*b* along with the experimental electron density map near the active site.

Ligand-dependent Subdomain Hinge-bending Movement—There is a clear difference between the native and inhibitor-bound ACE2 structures with respect to the distance separating the two subdomains (Fig. 4*A*). These two subdomains undergo a large inhibitor-dependent hinge-bending movement of one catalytic subdomain relative to the other (~16°) that causes the deep open cleft in the native form of the enzyme to close around the inhibitor. This movement can be viewed when subdomain II from the native and inhibitor-bound ACE2 structures are superimposed (root mean square (r.m.s.) deviation of 1.41 Å for 409 residues) as shown in Fig. 4*A*. In this view, subdomain II remains essentially unchanged, but subdomain I moves to close the gap, essentially mimicking the action of a closing clam shell. The α-carbon atoms of some residues near the outer edge of the subdomain gap move as much as ~13 Å, whereas residues lying near or on the hinge axis (residues 99 and 100, 284–293, 396 and 397, 409 and 410, 433 and 434, 539–548, and 564–568) are nearly stationary.

The movement of residues within the active site is shown in

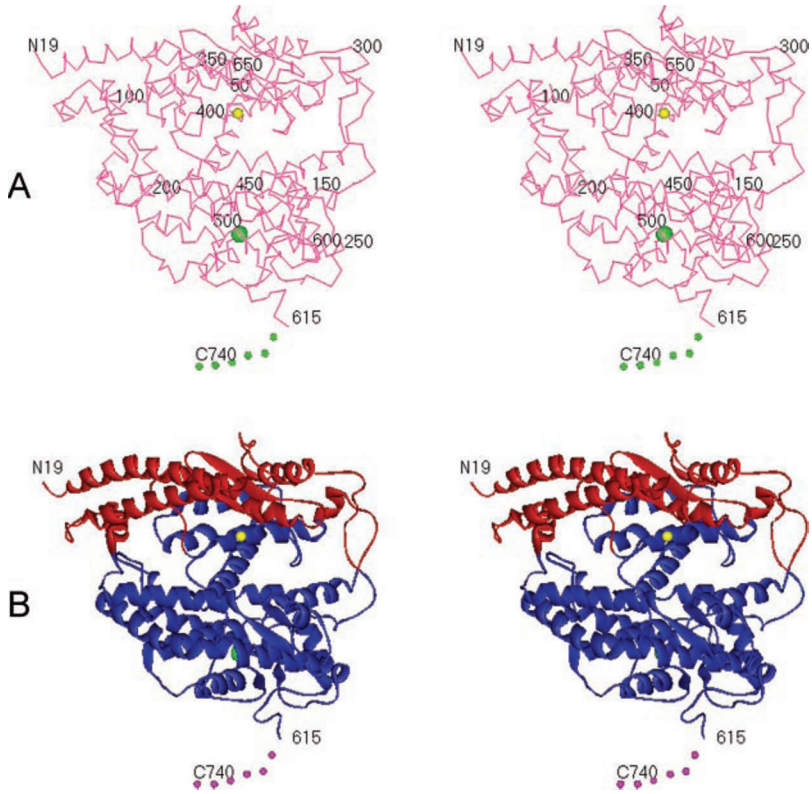

FIG. 3. **Overview of the native ACE2 crystal structure.** *A*, α-carbon trace of the native ACE2 structure looking down into the metallopeptidase active site cleft. The metallopeptidase catalytic domain is colored *red*. The active site zinc ion is shown as a *yellow sphere*, and the single bound chloride ion is shown as a *green sphere*. The S_1' subsite for inhibitor and substrate binding is to the right of the zinc ion, and the S_1 subsite is to the left. The collectrin homology domain at the C terminus is disordered and denoted by the *green dotted line*. *B*, ribbon diagram of native ACE2 showing the secondary structure and also the two subdomains (I and II) that form the two sides of the active site cleft. The two subdomains are defined as follows: the N terminus- and zinc-containing subdomain I (*red*), composed of residues 19–102, 290–397, and 417–430; and the C terminus-containing subdomain II (*blue*), composed of residues 103–289, 398–416, and 431–615. This definition is based on motion observed upon inhibitor binding (see Fig. 4). Zinc and chloride ions are denoted as described for *A*.

Fig. 4*B*. This view is a close-up of Fig. 4*A* with subdomain II of the native and inhibitor-bound ACE2 structures superimposed. Many of these residues move as much as 6–9 Å after binding of the inhibitor. Similar subdomain hinge-bending motions have also been observed for other zinc metalloproteases (29, 30). The largest previously observed ligand-dependent movement for metalloproteases is a 14° hinge-bending subdomain motion demonstrated for *Pseudomonas aeruginosa* elastase (open *versus* closed) that resulted in an ~2-Å movement to close the N-terminal/C-terminal subdomain gap (29). Domain closure movements in proteins are a common mechanism for the positioning of critical groups around substrates and inhibitors (31–33) and also for the trapping of substrate and reaction intermediates (34).

Inhibitor Binding Interactions and Implications for Substrate Specificity and Catalysis—Both metallopeptidase subdomains of ACE2 are nearly equally involved in binding of the inhibitor MLN-4760. Inspection of the interactions between MLN-4760 and ACE2 revealed important residues responsible for inhibitor binding and presumably for substrate binding and catalysis (Fig. 5). The inhibitor MLN-4760 has two carboxylate groups, one of which binds to the zinc atom by displacing the bound water molecule present in the native ACE2 structure. The zinc coordination sphere (His^{374}, His^{378}, and Glu^{402}) is a subset of the 21 residues of ACE2 that are located within 4.5 Å of the bound inhibitor and that make up the greater part of the active site. Six of the most important of these residues contribute specific H-bonding interactions with MLN-4760 (Fig. 5). The side chains of Arg^{273}, His^{505}, and His^{345} are H-bonded to the terminal carboxylate of the inhibitor. The carbonyl oxygen atom of Pro^{346} and the N-ϵ atom of His^{345} are within H-bonding distance of the secondary amine group of the inhibitor. Thr^{371} is within H-bonding distance of the imidazole ring of the 3,5-dichlorobenzylimidazole group of MLN-4760. The phenolic group of Tyr^{515} donates an H-bond to the zinc-bound carboxylate group of the inhibitor. The carboxyl group of Glu^{375} is within H-bonding distance of the other oxygen atom of the zinc-bound carboxylate of MLN-4760, but is presumably not protonated until peptide hydrolysis occurs (see below).

The zinc-bound carboxylate of MLN-4760 appears to mimic the zinc-bound tetrahedral intermediate characteristic of nucleophilic attack of the scissile bond by the zinc-bound water during peptide hydrolysis (35). This transition state structure is usually stabilized by H-bonds donated by imidazole, phenolic, or guanidino functional groups of neighboring amino acid side chains in other zinc metalloproteases (30, 35). For ACE2, this carboxyl anion stabilization most likely occurs through the phenolic group of Tyr^{515} (Fig. 5).

Besides the zinc coordination sphere and potential H-bond-contributing residues, there are an additional 11 residues of ACE2 that make close contacts (<4.5 Å) with MLN-4760, many of which are shown in Fig. 5. These residues do not contribute direct H-bonding interactions with the inhibitor, but provide important electrostatic and van der Waals interactions with MLN-4760. These residues define the S_1 and S_1' peptide-binding subsites, thereby providing the inhibitor, as well as substrate, binding specificity.

The isobutyl group of MLN-4760 packs nicely into the S_1 subsite of ACE2 (Fig. 5*A*), suggesting a similar preferred fit for a leucyl side chain at the P_1 position of peptide substrates. The topology and chemical environment of the S_1 subsite are dictated by four residues (Tyr^{510}, Arg^{514}, Phe^{504}, and Thr^{347}) that are expected to restrict the size of substrate P_1 side chains. Large substrate P_1 residues such as Trp, Tyr, Phe, Arg, and Lys would require significant movement of the phenolic side chain of Tyr^{510}, which forms a lid over the top of the S_1 subsite. This observation is consistent with the reported substrate specificity data showing only medium sized residues (Pro and Leu) at the P_1 position for preferred substrates with $k_{cat}/K_m > 10^5\ M^{-1}\ s^{-1}$ (8). Peptides with Phe and Tyr at the P_1 position, such as angiotensin-(1–9) (DRVYIHPFH), bradykinin (RPPGFSPFR), Leu-enkephalin (YGGFL), Met-enkephalin (YGGFM), and angiotensin-(1–5) (DRVYI), are not substrates for ACE2 despite the presence of preferred hydrophobic or basic P_1' resi-

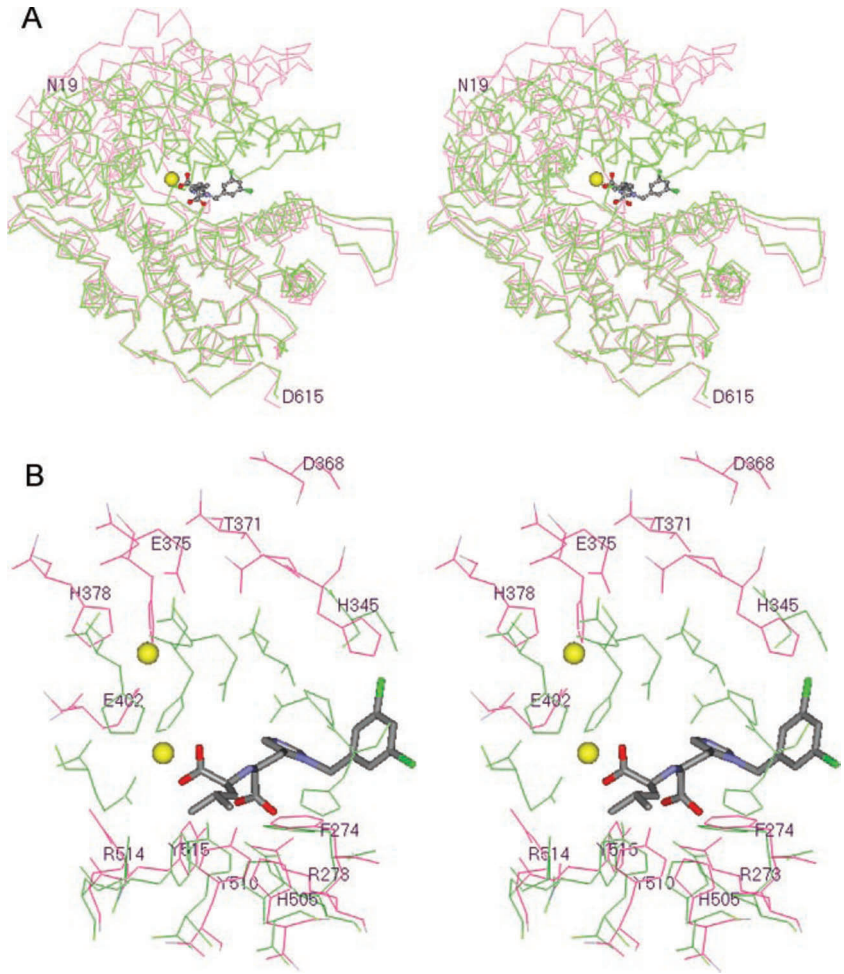

FIG. 4. **Superposition of the native and inhibitor-bound ACE2 structures.** *A*, the 409 α-carbon atoms corresponding to subdomain II of the native and inhibitor-bound ACE2 structures were superimposed with an r.m.s. deviation of 1.41 Å. Native ACE2 is colored *red*, and inhibitor-bound ACE2 is colored *green*. The zinc ion is shown as a *yellow sphere*, and the inhibitor MLN-4760 is shown in a *ball-and-stick* rendering with default atom coloring: *gray*, carbon; *blue*, nitrogen; *red*, oxygen; *green*, chlorine. This view is looking down the length of the active site cleft and is rotated 90° from that shown in Fig. 3. This perspective illustrates the ~16° hinge-bending movement of subdomain I relative to subdomain II that occurs upon inhibitor binding to ACE2. *B*, shown is a close-up view of the active sites of the superimposed native (*red*) and inhibitor-bound (*green*) ACE2 structures. This is the same superposition of subdomain II for both structures as described for *A*. In this perspective, the residues of subdomain I within the active site are shown to move upon inhibitor binding relative to those in subdomain II. The inhibitor MLN-4760 is shown in *stick* rendering with the same atom color code as described for *A*. The average movement for residues near the active site is 6–9 Å. The *yellow spheres* are the two positions of the zinc atom in the native and inhibitor-bound structures. This figure was prepared using MOE 2003.02 software (Chemical Computing Group, Inc.).

dues. Some ACE2-catalyzed hydrolysis was observed for peptides with a slightly larger residue (His) at the P_1 site (*i.e.* angiotensin I), but the catalytic efficiency was orders of magnitude lower (k_{cat}/K_m = 4.9 × 10^3 M^{-1} s^{-1}) despite good binding.

The limited size of the S_1 subsite may also account for the observed orientation of binding of MLN-4760. The design principles leading to the identification of MLN-4760 were based on assumptions from substrate screening studies and information regarding known metallopeptidase inhibitors (36). Consequently, MLN-4760 was designed as a His-Leu mimetic, in which the isobutyl side chain was predicted to mimic the Leu side chain (P_1'), and the substituted His was expected to bind in the S_1-S_2 subsites (15). Furthermore, the Leu carboxylate was envisioned to mimic the substrate's C-terminal carboxylate, and the His carboxylate was expected to coordinate the zinc atom. Although the inhibitor potency optimization was supported by this design hypothesis (several selective inhibitors at <10 nM), experimentally, the inhibitor-bound crystal structure reveals that MNL-4760 binds in the opposite orientation: the two carboxylates are reversed, the isobutyl side chain occupies the S_1 subsite, and the 3,5-dichlorobenzylimidazole group binds in the S_1' subsite. This alternative binding mode may be the result of the small S_1 subsite, which cannot accommodate the 3,5-dichlorobenzyl group. Models of MLN-4760 bound to ACE2 that were based on the tACE structure (37) did not predict the observed binding mode shown in Fig. 5. Retrospective comparison of the inhibitor structure-activity relationship with the crystal structure supports the unanticipated binding orientation. During the potency optimization studies, it appeared that the His portion of the inhibitors better tolerated changes in size and physicochemical properties compared with the Leu portion, which is consistent with the new experimental evidence (Fig. 5).

The S_1' subsite of ACE2 is much larger than the S_1 subsite and is formed by the lengthwise channel between the two subdomains. In addition to the aforementioned residues that contribute specific H-bonding interactions with MLN-4760 (Arg^{273}, His^{345}, His^{505}, Thr^{371}, and the carbonyl group of Pro^{346}), there are a number of other residues that make close contacts with the 3,5-dichlorobenzylimidazole group of the inhibitor. The side chains of Phe^{274}, Pro^{346}, Thr^{371}, Met^{360} and the disulfide linkage of Cys^{344} and Cys^{361} provide a hydrophobic environment for the S_1' subsite. Additional close contacts are observed for the side chains of Asp^{368}, Glu^{145}, Asn^{149}, and Lys^{363} and the carbonyl groups of Cys^{344} and Cys^{361}, which accommodate the far end of the dichlorobenzyl ring as depicted in Fig. 5*B*. The large size of the this S_1' subsite easily accommodates the 3,5-dichlorobenzylimidazole group of MLN-4760 and mirrors the observed preference for large hydrophobic or basic residues (Arg and Lys) at the P_1' position of peptide substrates (8).

Comparison with Structural Homologs—There are four proteins in the Protein Data Bank (38) that have overall architectural similarity to ACE2. They include the following: 1) the recently solved human tACE (code 1O86) (13), an enzyme of the M2 metallopeptidase family (EC 3.4.15.1); 2) *Drosophila* ACE (code 1J36), with which ACE2 shares ~35% sequence identity (14); 3) rat neurolysin (code 1I1I) (39), an M3 metallopeptidase family member (EC 3.4.24.16) with which ACE2 shares just

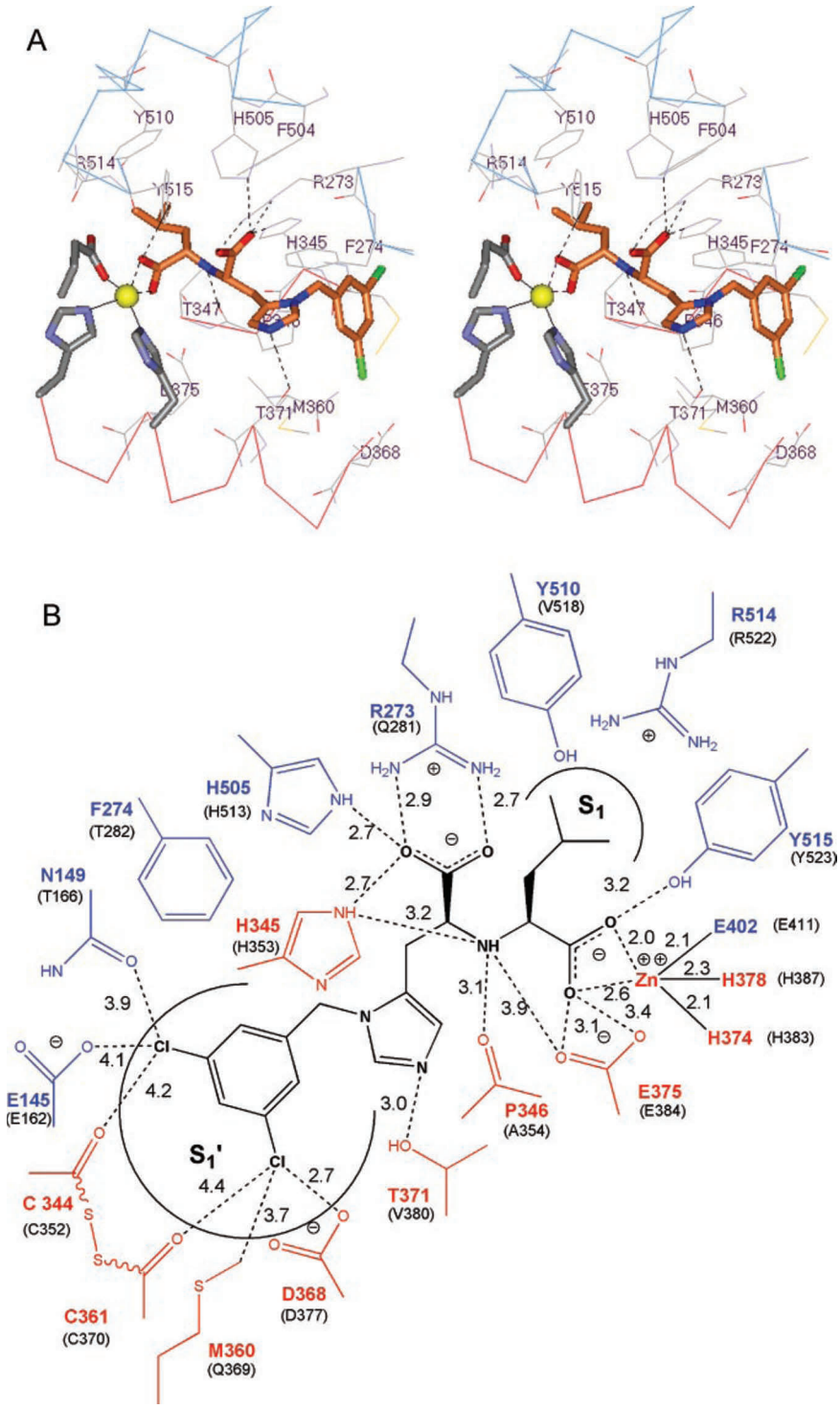

FIG. 5. **Binding interactions of the inhibitor MLN-4760 at the active site of ACE2.** *A*, the residues of ACE2 that contribute direct binding interactions with the inhibitor MLN-4760 are shown. MLN-4760 is shown in *stick* rendering with the same atom color code as described in the legend to Fig. 4*A*, except carbon is *orange*. The α-helix 11 segment derived from subdomain I has the α-carbon wire colored *red*, and turns and β-elements derived from subdomain II have the α-carbon wire colored *blue*. Probable H-bonding interactions are shown as *black dashed lines*. The zinc ion is shown as a *yellow sphere*. ACE2 residues coordinating the zinc ion are shown in *stick* rendering. *B*, shown is a schematic view of MLN-4760 binding interactions. MLN-4760 is shown in *black*. Residues derived from subdomain I are *red*, and residues derived from subdomain II are *blue*. The equivalent residues in tACE are in given in *parentheses*. Distances are measured in angstroms.

~17% sequence identity; and 4) *Pyrococcus furiosus* carboxypeptidase (code 1KA2) (40), a member of the M32 carboxypeptidase family.

Comparison with tACE—The α-carbon atoms of lisinopril-bound tACE were superimposed onto the equivalent atoms of inhibitor-bound ACE2 (588 residues) with an r.m.s. deviation of 1.80 Å (Fig. 6*A*), suggesting that these two protein structures are very similar. The largest difference between the ACE2 and tACE α-carbon traces is the insertion of a loop extension of 10 residues (Gly^{211}–Gly^{220}) between α-helices 7 and 8 in subdomain II of ACE2.

An improved superposition of the inhibitor-bound ACE2 and tACE structures (r.m.s. deviation of 0.53 Å) was obtained by considering just the equivalent α-carbon atoms of the aforementioned 21 residues of ACE2 that come within 4.5 Å of the bound MLN-4760 (Fig. 6*B*). Thirteen of these active site residues are conserved in the tACE and sACE enzymes: Glu^{145}, Cys^{344}, His^{345}, Cys^{361}, Asp^{368}, His^{374}, Glu^{375}, His^{378}, Glu^{402}, Phe^{504}, His^{505}, Arg^{514}, and Tyr^{515}. These structural similarities reflect the nearly identical way that MLN-4760 and lisinopril sit in the superimposed active sites (Fig. 6*B*).

The remaining eight active site ACE2 residues are substituted in tACE as follows: Asn^{149} → Thr, Arg^{273} → Gln, Pro^{346} → Ala, Thr^{347} → Ser, Met^{360} → Gln, Lys^{363} → Thr, Thr^{371} → Val, and Tyr^{510} → Val. These changes at the active sites of ACE2, tACE, and sACE presumably play a significant role in the observed

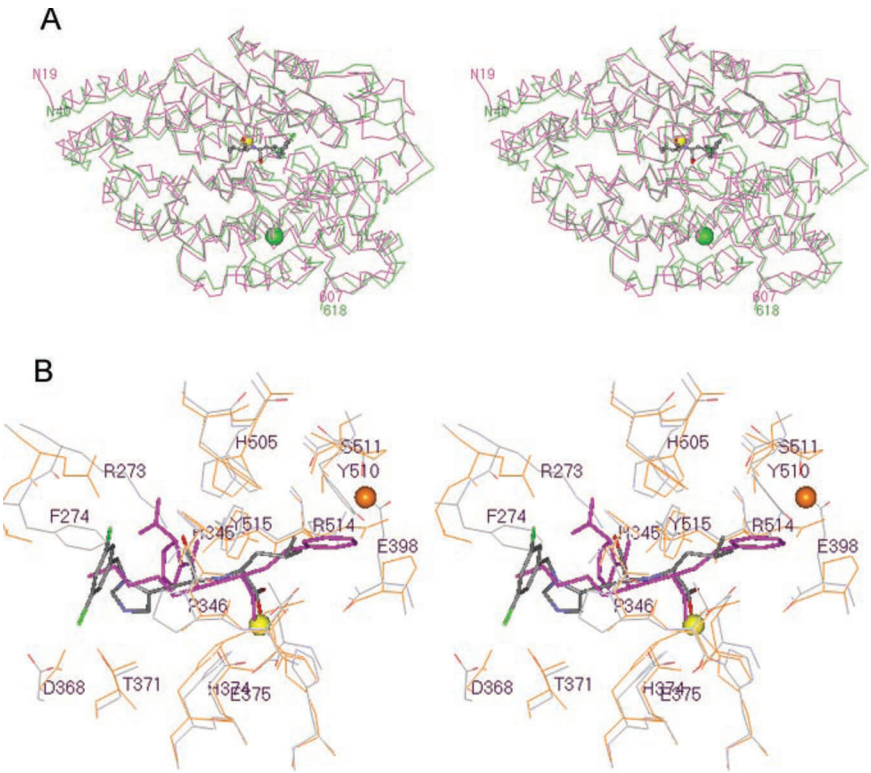

FIG. 6. **Superposition of the ACE2 and tACE structures.** *A*, the α-carbon atoms in lisinopril-bound tACE (13) were superimposed onto the equivalent atoms in inhibitor-bound ACE2 (588 residues) with an r.m.s. deviation of 1.80 Å. MLN-4760-bound ACE2 is *magenta*, and lisinopril-bound tACE is *green*. MLN-4760 is shown bound to ACE2 with the same color code described in the legend to Fig. 4*A*. Similarly, the zinc and chloride ions are shown as described in the legend to Fig. 3. The orientation is the same as that shown for native ACE2 in Fig. 3. Structures were superimposed using MOE 2003.02 software. *B*, the 21 α-carbon atoms at the inhibitor-bound active site of ACE2 (residues 4.5 Å from the inhibitor) were superimposed onto the equivalent atoms of lisinopril-bound tACE (Protein Data Bank code 1O86) with an r.m.s. deviation of 0.53 Å. The active site of ACE2 and MLN-4760 are shown in default colors, with the inhibitor displayed in *stick* rendering. Labels are for ACE2 residues only. The active site residues of tACE are shown in *orange*, with the inhibitor lisinopril colored *purple* in *stick* rendering. The zinc ion is shown as a *yellow sphere*, and the second chloride ion of tACE (CL2) is shown as an *orange sphere*. This chloride ion site does not exist in ACE2 due to the Glu^{398} substitution for Pro^{407} (see "Results and Discussion"). Other important differences between ACE2 and tACE are as follows: Arg^{273} *versus* Gln^{281}, Phe^{274} *versus* Thr^{282}, and Tyr^{510} *versus* Val^{518}, respectively.

differences in substrate specificity and inhibitor binding profiles for these homologous enzymes. As was discussed previously, Tyr^{510} and Thr^{347} line the S_1 subsite of ACE2 and confine this subsite for the accommodation of only small and medium sized side chains such as leucyl and prolyl, which is consistent with the known substrate preferences (8). The smaller side chains at the S_1 subsite of tACE make this subsite somewhat larger in tACE than observed for ACE2. In a superposition of the inhibitor-bound ACE2 and lisinopril-bound tACE structures, the Tyr^{510} phenolic group of ACE2 occupies the space where the P_1 phenylpropyl group of the lisinopril resides (Fig. 6*B*).

Another important difference between ACE2 and tACE is the $Arg^{273} \rightarrow Gln$ substitution. The guanidino group of Arg^{273} makes a bidentate H-bond with the terminal carboxylate of MLN-4760 (Fig. 5). Not only does the guanidino group of Arg^{273} stabilize the terminal carboxylate of the inhibitors and peptide substrates, but its larger size (compared with Gln in tACE) causes steric crowding at the potential S_2' binding subsite. The superposition of lisinopril-bound tACE onto MLN-4760-bound ACE2 reveals that the guanidino group of Arg^{273} nearly superimposes on the terminal carboxylate of the P_2' Pro residue of lisinopril, thereby severely limiting the size of the S_2' subsite in ACE2 compared with tACE (Fig. 6*B*). This single residue difference in ACE2 relative to tACE essentially eliminates the S_2' subsite in ACE2 and offers an explanation for the observed switch in the peptidyl dipeptidase activity of tACE to the observed carboxypeptidase activity of ACE2. This difference at the S_1' and S_2' subsites for the homologous enzymes also helps to clarify why the potent ACE inhibitors lisinopril, enalaprilat, and captopril are inactive against ACE2 (2).

The native tACE structure was reported to be nearly identical to the lisinopril-bound tACE structure (13), suggesting that no ligand-dependent conformational change occurs for tACE or at least under the conditions used to obtain these crystals (pH 4.7, 50 mM sodium acetate with an unspecified [Cl^-]) (41). However, inspection of the reported native tACE structure (Protein Data Bank code 1O8A) reveals that two ligands are bound to the active site: an acetate molecule bound to the zinc atom and an unknown compound that presumably originated during protein expression and purification. This compound was modeled as an *N*-carboxyalanine and is isosteric with 2-methylsuccinic acid according to notes deposited with the native tACE coordinates in the Protein Data Bank file. This 2-methylsuccinate-like ligand is bound to tACE in a manner that closely resembles that observed for lisinopril. Five of the same H-bonds present in the lisinopril-bound tACE structure are also present for the 2-methylsuccinate-like ligand. Therefore, the reported native tACE structure would appear to be another ligand-bound structure, and its closed conformational state is consistent with other ligand-bound tACE and ACE2 structures.

Structural Homology for the Catalytic Motif—ACE2 and related ACE enzymes are related to other HE*XX*H clan members through divergent evolution with an overall primary sequence identity that is <15% (Fig. 7*A*). The two largest metallopeptidase clans are clan MA (gluzincin family) and clan MB, which include the many families of zinc metallopeptidases that have

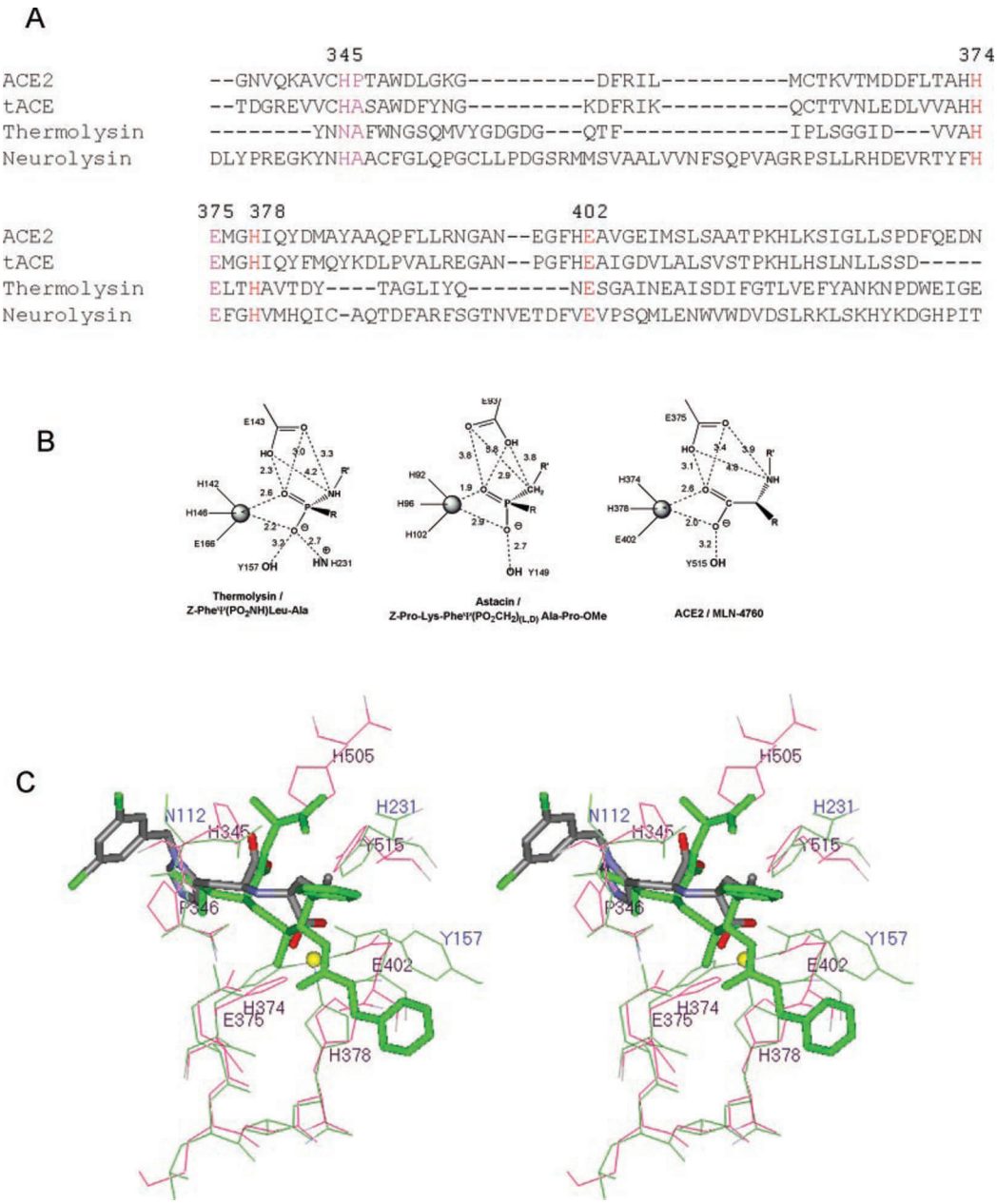

FIG. 7. **Structural homology for the ACE2 catalytic motif to other members of the HE*XX*H metallopeptidase clans.** *A*, shown is the structure-based sequence alignment of ACE2, tACE, thermolysin, and neurolysin. The conserved residues correspond to the catalytic motif for these enzymes (colored *red* (zinc binding) and *magenta*). Sequence numbering is for ACE2. *B*, the catalytic motifs for thermolysin and astacin bound to transition state analogs Z-PheΨ(PO$_2$NH)-Leu-Ala and Z-Pro-Lys-PheΨ(PO$_2$CH$_2$)-DL-Ala-Pro-OMe, respectively (30, 42), are compared with the ACE2 complex with MLN-4760. Distances are measured in angstroms. *C*, shown is the superposition of the catalytic motifs of ACE2 (*red*) and thermolysin (*green*). Eight α-carbon atoms corresponding to residues 345, 346, 374–378, and 402 of MLN-4760 bound ACE2 were superimposed onto the equivalent α-carbon atoms of Z-Pro-Lys-PheΨ(PO$_2$CH$_2$)-DL-Ala-Pro-OMe-bound thermolysin (see sequence alignment in *A*) with an r.m.s. deviation of 0.49 Å. Bound inhibitors are shown in *stick* rendering with default atom coloring for MLN-4760 and *green* coloring for Z-Pro-Lys-PheΨ(PO$_2$CH$_2$)-DL-Ala-Pro-OMe. The zinc ion is shown as a *yellow sphere*. ACE2 labels are *black*, and thermolysin labels are *blue*. Ψ indicates replacement of the peptide bond by the group in parentheses.

the HE*XX*H + E and HE*XX*H + H zinc-binding motifs, respectively (28). Among these clans, there is structural homology for the catalytic motif and the core of the inhibitor/substrate-binding site. Representative examples of the catalytic motifs of some members of these clans are shown in Fig. 7*B*. These active sites include thermolysin (clan MA) and astacin (clan MB) in complex with transition state analogs (30, 42). The ACE2 complex with MLN-4760 is shown for comparison. These transition state analogs bind to thermolysin and astacin in a manner that is similar to the way MLN-4760 binds to ACE2 and reveal a high level of structural homology between the catalytic motifs of these enzymes. Indeed, eight α-carbon atoms corresponding to residues 345, 346, 374–378, and 402 of MLN-4760-bound ACE2 were superimposed on equivalent α-carbon atoms of Z-Pro-Lys-PheΨ(PO$_2$CH$_2$)-DL-Ala-Pro-OMe-bound thermolysin with an r.m.s. deviation of 0.49 Å (Fig. 7*C*). This structural conservation of the key residues and scaffold is believed to translate into a preservation of the catalytic role of many elements of this motif.

Proposed Catalytic Mechanism for ACE2-mediated Peptide Hydrolysis—The strong structural homology of the active site of inhibitor-bound ACE2 to catalytic motifs of evolutionarily related enzymes in metallopeptidase clans MA and MB (Fig. 7) suggests that many of these structural elements play similar

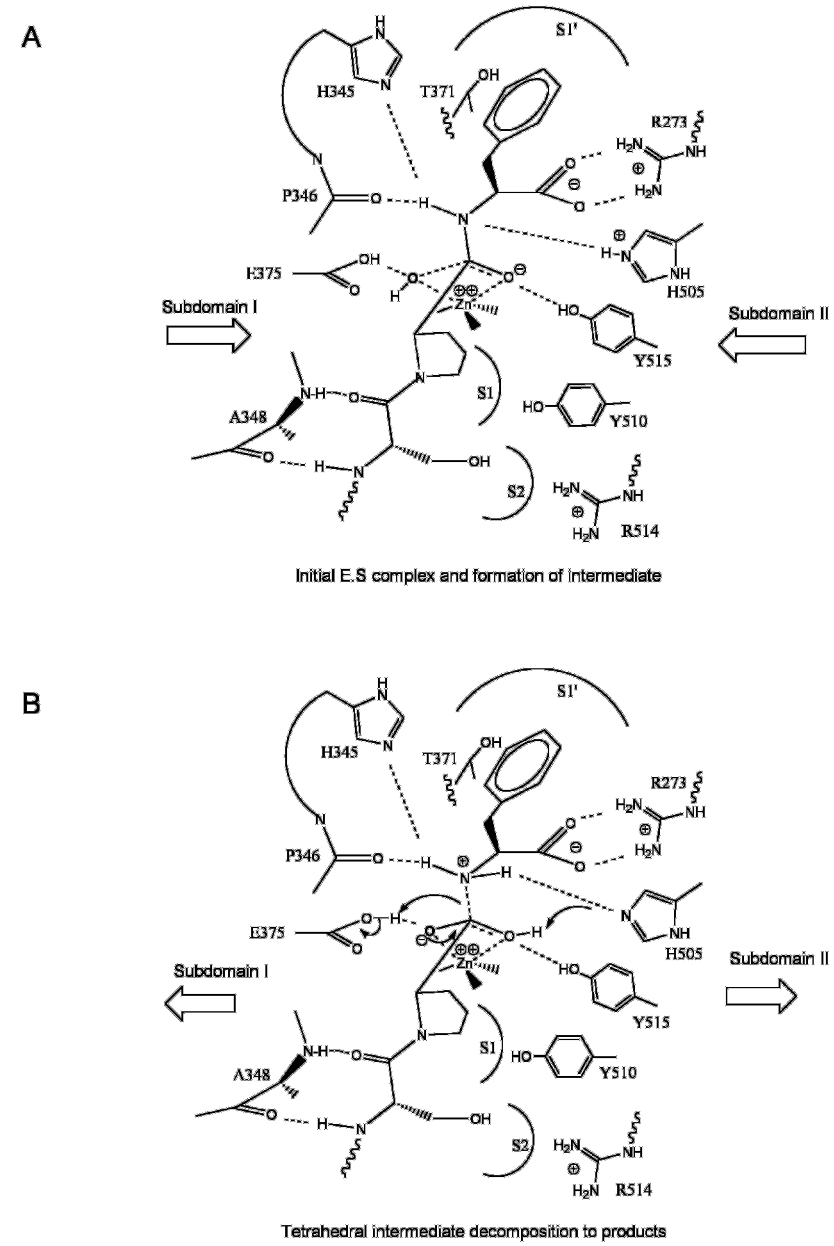

FIG. 8. **Proposed mechanism for ACE2-catalyzed hydrolysis of peptide substrates.** *A*, shown is the *ES* complex and progression to the tetrahedral intermediate. Substrate binding to one subdomain induces a subdomain hinge-bending movement (indicated by *large arrows*) to close the active site cleft and to bring important residues into position for catalysis. This movement is followed by attack of a zinc-bound water at the carbonyl group of the scissile amide bond to form a tetrahedral intermediate, resulting in transfer of a proton from the attacking water to Glu^{375} (35). Simultaneously, a proton is transferred from His^{505} to the leaving nitrogen atom of the P_1' residue. This sp^3 hybridized nitrogen is stabilized by H-bonds from Pro^{346}, His^{505}, and/or His^{345}. *B*, collapse of the tetrahedral intermediate to the products occurs by breaking of the amide C–N bond together with abstraction of a proton from Glu^{375} by the emerging free nitrogen of the product amino acid. The new emerging product carboxyl group can then transfer a proton back to His^{505} either directly by exchange between carboxyl oxygen atoms or by exchange with solvent.

catalytic roles in ACE2. These similarities have led to a proposed catalytic mechanism for ACE2 (Fig. 8) that has many features in common with mechanisms proposed for other HE*XX*H zinc metallopeptidase clan members (30, 35, 40). The mechanism reveals a probable initial *ES* complex formation and generation of the tetrahedral intermediate. The formation of this *ES* complex causes an ~16° subdomain hinge-bending movement of subdomain I toward subdomain II, bringing all the catalytic components into a functional orientation. These substrate and inhibitor-dependent subdomain movements are consistent with induced fit and transition state theories of catalysis (43).

Other metallopeptidases exhibit hinge-bending motions upon ligand binding (see above), but the average ligand-dependent displacements of 6–9 Å for residues at the active site of ACE2 (Fig. 4*B*) are much larger than previously reported displacements (~2 Å) (29). These relative movements at the active site of metallopeptidases are a function of the hinge-bending angle and also the size of the opposing subdomains. Another distinguishing feature of this mechanism is the proton transfer from His^{505} to the leaving nitrogen atom of the P_1' residue. A protonated histidine is supported by the pH-rate profile that has a maximum at 6.5 (8). Additional evidence for the role for His^{505} comes from site-directed mutagenesis in sACE, where mutation of the analogous His^{1089} to Ala results in a 100-fold drop in k_{cat} and 4.5-fold drop in K_m (44). Similarly, the $His^{1089} \rightarrow$ Leu mutation results in a 671-fold drop in k_{cat} and a 6.2-fold drop in K_m. The much larger impact on k_{cat} compared with K_m supports a catalytic role for this histidine rather than an important binding function (44). His^{505} appears to be too far from the zinc-bound carboxylate (6.3 Å) to be directly involved in H-bonding stabilization of the carbonyl tetrahedral intermediate, as was expected from sequence homology (44). Protonation and stabilization of the sp^3 hybridized nitrogen of the peptide intermediate as depicted in Fig. 8 may better explain the site-directed mutagenesis data. Many elements of this mechanism are believed to be relevant to tACE and sACE as well, except with release of dipeptide products due to the larger, more accommodating S_2' subsite in ACE.

Anion-binding Sites—An interesting aspect of the ACE2-mediated substrate hydrolysis is the activation by chloride ions and other anions (8) in much the same way that anions activate

substrate hydrolysis and inhibitor binding for sACE and tACE (45, 46). A single bound chloride ion was identified in the high resolution native ACE2 structure (Fig. 3). The location of this anion-binding site in subdomain II is nearly identical to the position of a chloride ion in the tACE structure, which was designated CL1 (13). The chloride-coordinating ligands Arg^{169}, Trp^{477}, and Lys^{481} correspond to Arg^{186}, Trp^{485}, and Arg^{489}, respectively, in tACE. In ACE2, this anion-binding site is ~21 Å away from the active site zinc ion and ~16 Å away from the dichlorobenzyl group of bound MLN-4760. A second chloride-binding site was identified for tACE (designated CL2) and found to be composed of coordinating side chains from Arg^{522} and Tyr^{224} and bracketed by Pro^{407} and Pro^{519} on two sides. Arg^{522} and Tyr^{227} are conserved in ACE2 as Arg^{514} and Tyr^{207}, but the two bracketing proline residues are replaced in ACE2 with Glu^{398} and Ser^{511}, respectively. This double substitution has the effect of eliminating the CL2 anion-binding site in ACE2 because it causes the projection of Glu and Ser side chains into the location of where CL2 binds to tACE (Fig. 6*B*).

With only a single common anion-binding site observed for ACE2 and tACE (CL1), it is possible to imagine that this site is responsible for the anion activation effect in both homologous enzymes. On the other hand, site-directed mutagenesis studies suggest that the Cl^--coordinating ligand Arg^{1098} of sACE (Arg^{522} of tACE) at the second chloride ion site in tACE (CL2) plays a role in anion activation in sACE (47). The equivalent residue in ACE2 (Arg^{514}) cannot play the same role because this chloride-binding site is replaced in ACE2 with the Glu^{398}/Ser^{511} double substitution.

A simple explanation for the experimentally observed anion activation in ACE2 is that a second chloride ion site exists in substrate- or inhibitor-bound ACE2, but at a different location than observed for tACE. This second anion-binding site, specific to the inhibitor-bound form of the enzyme, may help to shift the open/closed conformational equilibrium in favor of the closed or catalytic competent closed conformer, thus ensuring a tighter grasp on the transition state for peptide hydrolysis. Kinetic models for the effect of anions on the activity and inhibition of sACE (45, 46) are consistent with chloride ions influencing catalysis through shifts in conformer equilibria. Unfortunately, the lower resolution of the MLN-4760-bound ACE2 structure (3.0 Å) limits the distinction between chloride ions and water molecules in this model. One or more of the 13 water molecules modeled into the inhibitor-bound ACE2 structure could be additional bound chloride ions, but higher resolution data are needed to confirm. Similarly, it is not known whether the second chloride ion of tACE (CL2) is unique to inhibitor-bound tACE and not bound in native tACE because no true native tACE structure is currently available.

ACE2 as the SARS Coronavirus Receptor—The recent identification of ACE2 as a functional receptor for the SARS coronavirus (4, 5) has raised questions about what binding determinants on ACE2 interact with the virus. Mutations of the ACE2 zinc-coordinating residues His^{374} and His^{378} to asparagines were found to have no effect on syncytial formation (4), suggesting that interfering with the active site has no effect on viral spike protein binding to ACE2. However, the large conformational change observed upon MLN-4760 binding to ACE2 could prove to be unfavorable for viral binding to its receptor and/or syncytial formation. Thus, metallopeptidase inhibitors such as MLN-4760 may still prove useful for prevention of viral binding to ACE2 and blockage of infection. The ACE2 structures reported here are expected to be useful in aiding efforts to identify the binding site for the SARS coronavirus spike protein. Moreover, the x-ray structures should enable the future design of more potent and specific inhibitors of ACE2, at either the metallopeptidase site or any separate viral spike protein-binding exosite that may be discovered.

Acknowledgments—We thank Rebecca Matthew and Geoff Stamper for help with the characterization of early ACE2 crystals and Larry Dick, Paul Hales, Chad Vickers, Peter Tummino, Mary Donoghue, and Susan Acton for many discussions regarding the characterization of ACE2. We are grateful to Kazumi Shiosaki, Julian Adams, Andrew Nichols, and Michael Kuranda for support.

REFERENCES

1. Donoghue, M., Hsieh, F., Baronas, E., Godbout, K., Gosselin, M., Stagliano, N., Donovan, M., Woolf, B., Robison, K., Jeyaseelan, R., Breitbart, R. E., and Acton, S. (2000) *Circ. Res.* **87,** E1–E9
2. Tipnis, S. R., Hooper, N. M., Hyde, R., Karran, E., Christie, G., and Turner, A. J. (2000) *J. Biol. Chem.* **275,** 33238–33243
3. Crackower, M. A., Sarao, R., Oudit, G. Y., Yagil, C., Kozieradzki, I., Scanga, S. E., Oliveira-dos-Santos, A. J., da Costa, J., Zhang, L., Pei, Y., Scholey, J., Ferrario, C. M., Manoukian, A. S., Chappell, M. C., Backx, P. H., Yagil, Y., and Penninger, J. M. (2002) *Nature* **417,** 822–828
4. Li, W., Moore, M. J., Vasilieva, N., Sui, J., Wong, S. K., Berne, M. A., Somasundaran, M., Sullivan, J. L., Luzuriaga, K., Greenough, T. C., Choe, H., and Farzan, M. (2003) *Nature* **426,** 450–454
5. Xiao, X., Chakraborti, S., Dimitrov, A. S., Gramatikoff, K., and Dimitrov, D. S. (2003) *Biochem. Biophys. Res. Commun.* **312,** 1159–1164
6. Krege, J. H., John, S. W., Langenbach, L. L., Hodgin, J. B., Hagaman, J. R., Bachman, E. S., Jennette, J. C., O'Brien, D. A., and Smithies, O. (1995) *Nature* **375,** 146–148
7. Esther, C. R., Jr., Howard, T. E., Marino, E. M., Goddard, J. M., Capecchi, M. R., and Bernstein, K. E. (1996) *Lab. Investig.* **74,** 953–965
8. Vickers, C., Hales, P., Kaushik, V., Dick, L., Gavin, J., Tang, J., Godbout, K., Parsons, T., Baronas, E., Hsieh, F., Acton, S., Patane, M., Nichols, A., and Tummino, P. (2002) *J. Biol. Chem.* **277,** 14838–14843
9. Schechter, I., and Berger, A. (1967) *Biochem. Biophys. Res. Commun.* **27,** 157–162
10. Turner, A. J., and Hooper, N. M. (2002) *Trends Pharmacol. Sci.* **23,** 177–183
11. Danilczyk, U., Eriksson, U., Crackower, M. A., and Penninger, J. M. (2003) *J. Mol. Med.* **81,** 227–234
12. Oudit, G. Y., Crackower, M. A., Backx, P. H., and Penninger, J. M. (2003) *Trends Cardiovasc. Med.* **13,** 93–101
13. Natesh, R., Schwager, S. L., Sturrock, E. D., and Acharya, K. R. (2003) *Nature* **421,** 551–554
14. Kim, H. M., Shin, D. R., Yoo, O. J., Lee, H., and Lee, J. O. (2003) *FEBS Lett.* **538,** 65–70
15. Dales, N. A., Gould, A. E., Brown, J. A., Calderwood, E. F., Guan, B., Minor, C. A., Gavin, J. M., Hales, P., Kaushik, V. K., Stewart, M., Tummino, P. J., Vickers, C. S., Ocain, T. D., and Patane, M. A. (2002) *J. Am. Chem. Soc.* **124,** 11852–11853
16. Hauptman, H. A. (1997) *Methods Enzymol.* **277,** 3–13
17. Abrahams, J. P., and de Graaff, R. A. (1998) *Curr. Opin. Struct. Biol.* **8,** 601–605
18. Bricogne, G., Vonrhein, C., Flensburg, C., Schiltz, M., and Paciorek, W. (2003) *Acta Crystallogr. Sect. D Biol. Crystallogr.* **59,** 2023–2030
19. Otwinowski, Z. (1991) in *Isomorphous Replacement and Anomalous Scattering*: *Proceedings of the CCP4 Study Weekend*, (Wolf, W., Evans, P. R., and Leslie, A. G. W., eds) pp. 80–86, Daresbury Laboratory, Warrington, United Kingdom
20. McRee D. E. (1999) *Practical Protein Crystallography*, 2nd Ed., Academic Press, Inc., San Diego, CA
21. Navaza, J., and Saludjian, P. (1997) *Methods Enzymol.* **276,** 581–594
22. Brunger, A. T., Adams, P. D., Clore, G. M., DeLano, W. L., Gros, P., Grosse-Kunstleve, R. W., Jiang, J. S., Kuszewski, J., Nilges, M., Pannu, N. S., Read, R. J., Rice, L. M., Simonson, T., and Warren, G. L. (1998) *Acta Crystallogr. Sect. D Biol. Crystallogr.* **54,** 905–921
23. Zhang, H., Wada, J., Hida, K., Tsuchiyama, Y., Hiragushi, K., Shikata, K., Wang, H., Lin, S., Kanwar, Y. S., and Makino, H. (2001) *J. Biol. Chem.* **276,** 17132–17139
24. Fulop, V., Bocskei, Z., and Polgar, L. (1998) *Cell* **94,** 161–170
25. Rockel, B., Peters, J., Kuhlmorgen, B., Glaeser, R. M., and Baumeister, W. (2002) *EMBO J.* **21,** 5979–5984
26. Pantoliano, M. W., Holmquist, B., and Riordan, J. F. (1984) *Biochemistry* **23,** 1037–1042
27. Bernstein, K. E., Welsh, S. L., and Inman, J. K. (1990) *Biochem. Biophys. Res. Commun.* **167,** 310–316
28. Rawlings, N. D., and Barrett, A. J. (1995) *Methods Enzymol.* **248,** 183–228
29. Holland, D. R., Tronrud, D. E., Pley, H. W., Flaherty, K. M., Stark, W., Jansonius, J. N., McKay, D. B., and Matthews, B. W. (1992) *Biochemistry* **31,** 11310–11316
30. Grams, F., Dive, V., Yiotakis, A., Yiallouros, I., Vassiliou, S., Zwilling, R., Bode, W., and Stocker, W. (1996) *Nat. Struct. Biol.* **3,** 671–675
31. Gerstein, M., Lesk, A. M., and Chothia, C. (1994) *Biochemistry* **33,** 6739–6749
32. Gerstein, M., and Krebs, W. (1998) *Nucleic Acids Res.* **26,** 4280–4290
33. Teague, S. J. (2003) *Nat. Rev. Drug Discov.* **2,** 527–541
34. Knowles, J. R. (1991) *Philos. Trans. R. Soc. Lond. Ser. B Biol. Sci.* **332,** 115–121
35. Matthews, B. W. (1988) *Acc. Chem. Res.* **21,** 333–340
36. Patchett, A. A., Harris, E., Tristram, E. W., Wyvratt, M. J., Wu, M. T., Taub, D., Peterson, E. R., Ikeler, T. J., ten Broeke, J., Payne, L. G., Ondeyka, D. L., Thorsett, E. D., Greenlee, W. J., Lohr, N. S., Hoffsommer, R. D., Joshua, H., Ruyle, W. V., Rothrock, J. W., Aster, S. D., Maycock, A. L.,

Robinson, F. M., Hirschmann, R., Sweet, C. S., Ulm, E. H., Gross, D. M., Vassil, T. C., and Stone, C. A. (1980) *Nature* **288,** 280–283
37. Guy, J. L., Jackson, R. M., Acharya, K. R., Sturrock, E. D., Hooper, N. M., and Turner, A. J. (2003) *Biochemistry* **42,** 13185–13192
38. Berman, H. M., Westbrook, J., Feng, Z., Gilliland, G., Bhat, T. N., Weissig, H., Shindyalov, I. N., and Bourne, P. E. (2000) *Nucleic Acids Res.* **28,** 235–242
39. Brown, C. K., Madauss, K., Lian, W., Beck, M. R., Tolbert, W. D., and Rodgers, D. W. (2001) *Proc. Natl. Acad. Sci. U. S. A.* **98,** 3127–3132
40. Arndt, J. W., Hao, B., Ramakrishnan, V., Cheng, T., Chan, S. I., and Chan, M. K. (2002) *Structure* **10,** 215–224
41. Gordon, K., Redelinghuys, P., Schwager, S. L., Ehlers, M. R., Papageorgiou, A. C., Natesh, R., Acharya, K. R., and Sturrock, E. D. (2003) *Biochem. J.* **371,** 437–442
42. Holden, H. M., Tronrud, D. E., Monzingo, A. F., Weaver, L. H., and Matthews, B. W. (1987) *Biochemistry* **26,** 8542–8553
43. Kraut, J. (1988) *Science* **242,** 533–540
44. Fernandez, M., Liu, X., Wouters, M. A., Heyberger, S., and Husain, A. (2001) *J. Biol. Chem.* **276,** 4998–5004
45. Shapiro, R., Holmquist, B., and Riordan, J. F. (1983) *Biochemistry* **22,** 3850–3857
46. Shapiro, R., and Riordan, J. F. (1984) *Biochemistry* **23,** 5234–5240
47. Liu, X., Fernandez, M., Wouters, M. A., Heyberger, S., and Husain, A. (2001) *J. Biol. Chem.* **276,** 33518–33525
48. Soubrier, F., Alhenc-Gelas, F., Hubert, C., Allegrini, J., John, M., Tregear, G., and Corvol, P. (1988) *Proc. Natl. Acad. Sci. U. S. A.* **85,** 9386–9390
49. Ehlers, M. R., Fox, E. A., Strydom, D. J., and Riordan, J. F. (1989) *Proc. Natl. Acad. Sci. U. S. A.* **86,** 7741–7745
50. Higgins, D. G., Thompson, J. D., and Gibson, T. J. (1996) *Methods Enzymol.* **266,** 383–402
51. Frishman, D., and Argos, P. (1995) *Proteins* **23,** 566–579